PHYSICAL REVIEW B **88**, 035203 (2013)

Strain-induced incommensurate distortions in epitaxial Ruddlesden-Popper-type Ba_2TiO_4

William D. Parker[1,2] and S. M. Nakhmanson[3]
[1]*Argonne Leadership Computing Facility, Argonne National Laboratory, Argonne, Illinois 60439, USA*
[2]*School of Chemical Engineering, Purdue University, West Lafayette, Indiana 47907, USA*
[3]*Department of Materials Science & Engineering, and Institute of Materials Science, University of Connecticut, Storrs, Connecticut 06269, USA*

(Received 27 March 2013; revised manuscript received 4 June 2013; published 15 July 2013)

With the help of first-principles-based computational techniques, we evaluate the structural, vibrational, and polar properties of a fictitious Ruddlesden-Popper-type Ba_2TiO_4 compound that is subjected to a range of epitaxial strains. We demonstrate that, depending on the value of the applied strain, this compound exhibits different types of incommensurate distortions, which does not happen in the similar, but better cation-size-balanced, Ca- and Sr-based structures. Furthermore, at moderate tensile strains this material develops spontaneous polarization (0.17 C/m^2 at 1.5% strain) that is directed along the perovskite planes. By virtue of having the same symmetry, planar incommensurate and polar distortions can interact with each other, which results in a variety of complicated ground-state structural arrangements whose properties could be fine tuned by epitaxial strain engineering.

DOI: 10.1103/PhysRevB.88.035203 PACS number(s): 77.84.−s, 77.80.bn, 63.22.Np, 81.05.Zx

I. INTRODUCTION

Although a variety of layered-oxide $A_{n+1}Ti_nO_{3n+1}$ Ruddlesden-Popper (RP) compounds[1,2] are known to exist either in crystalline[3,4] or in thin-film form,[5,6] this does not include any Ba-based structures. In fact, simple bond-strength analysis suggests that such materials cannot be produced, due to a large size disparity between the Ba and Ti cations.[7] A better cation-size-balanced Ba_2ZrO_4 structure actually forms as a RP-type compound,[7] and is a strong molecular absorber.[8,9] Ba_2TiO_4, however, crystallizes in the monoclinically distorted β-K_2SO_4-type structure (β-barium orthotitanate, space group $P2_1/n$;[10,11] a high-temperature orthorhombic α' phase, space group $P2_1nb$, also exists[12]) with, unique among other titanates, a tetrahedral, rather than octahedral, environment for the Ti ions. This phase, which can be produced as a ceramic[13–16] or a thin film,[17,18] also appears to have sizable molecular absorption properties and has been recently evaluated as a prospective material for high-temperature (550 °C and above) CO_2 capture.[19–21] $Ba_{2-x}Sr_xTiO_4$ solid solutions synthesized by a variety of ceramic techniques have also been investigated; however, a single-phase RP compound with any substantial concentration of Ba could not be made.[22,23]

The capability to absorb small molecules, demonstrated by RP Ba_2ZrO_4 and β-Ba_2TiO_4, but not the other RP-type perovskites (e.g., Sr or Ca based), is intriguing—that is, in addition to being useful for a range of possible applications. Initial experimental work[8,9,19–21] suggests that both materials can reversibly move large amounts of guest molecules, like CO_2 and water, through their bulk, undergoing dramatic structural transformations in the process. The physical underpinnings of this behavior are completely unknown, as multiple important questions, such as (i) where and how do adsorbates enter the solid, (ii) how exactly do they bind and move through it, and (iii) what structural and chemical changes take place inside the solid during the molecular loading-unloading cycle, remain unanswered. Currently, one can only *speculate* that, compared with similar layered materials based on Sr and Ca, due to the largeness of Ba ions these structures possess more open geometries, which may be connected to the observed unusual properties. Many of the structurally and chemically related oxides are so-called *functional materials,* i.e., their properties can be tuned by an applied external influence, such as an electric or a stress field. Therefore, gaining a better insight into the nature of molecular interactions with or inside their bulk forms could lead to emergence of novel functional absorbers with controllable behavior on the microscale. In this regard, achieving a *confluence* of good molecular absorption properties (selectivity, storage volume, and loading-unloading rates, as well as chemical stability and structure regeneration during multiple loading-unloading cycles) with tunable ferroic properties looks especially attractive.

If a RP phase of Ba_2TiO_4 were to be synthesized, it could inherit a number of the aforementioned traits from its next-of-kin compounds—ferroelectric perovskite $BaTiO_3$,[24] dielectric[25,26] and thermoelectric[27–30] Sr-based RP series, and the molecular absorbers RP Ba_2ZrO_4 and β-Ba_2TiO_4—potentially producing the right mixture of advanced functionalities. Modern state-of-the-art epitaxial engineering techniques, such as molecular beam epitaxy, offer an alternative avenue to avoid the restrictions imposed by bulk thermodynamics during growth: they can stabilize metastable structures through artificial elastic boundary conditions (misfit strain) and/or rate-limited kinetics.[31] In this study, we use first-principles density-functional theory (DFT) calculations to assess the structural stability and evaluate the polar and dielectric properties of the hypothetical RP Ba_2TiO_4 phase grown on a square substrate for a range of applied biaxial strains. We *do not* probe for the presence of potential elastic anomalies in the RP structure, assuming that the epitaxial growth condition will enforce its tetragonal symmetry, at least in relatively thin layers. Our investigation reveals that, unlike better cation-size-balanced Ca- or Sr-based RP structures, Ba_2TiO_4 exhibits an assortment of incommensurate distortions, including those that couple with in-plane polarization, and that competition between various distortion trends can be influenced by applying the right amount of epitaxial strain. The electronic, vibrational, and (supposedly high) dielectric properties[13] of the β-Ba_2TiO_4 phase are being explored by us as a separate project.[32]

The examination of the properties of both RP (this article) and β (Ref. 32) phases of Ba_2TiO_4 shows that, by virtue of its perovskitelike structure, the former compound exhibits a much stronger polar behavior. The expected confluence of molecular-absorption and ferroic functionalities in the RP phase could provide tantalizing glimpses into new kinds of *swing processes*—such as a ferroelectric one—for regenerative capture and release of small molecules. Most currently utilized approaches to molecular absorption and desorption involve the usage of temperature and/or pressure swing cycles, with CO_2 capture serving as a good example.[33] However, augmenting or completely replacing such "pristine" processes with those relying on ferroelectric switching or other ferroic properties may, among other potential enhancements, greatly improve their energy efficiency, opening up new avenues to more affordable and flexible molecular capture technology in the future.

II. COMPUTATIONAL DETAILS

DFT calculations were performed using the QUANTUM ESPRESSO package[34] within the local density approximation (LDA), parametrized by Perdew and Zunger.[35] The electronic wave functions (density) were expanded in plane waves up to 30 Ry (300 Ry), and the core and valence electrons were treated with Vanderbilt ultrasoft[36] pseudopotentials. $6 \times 6 \times 2$ and $6 \times 6 \times 4$ Monkhorst-Pack[37] meshes were used for the Brillouin zone (BZ) integrations and for phonon-band calculations, respectively, utilizing tetragonal $P4/mmm$ unit cells with two Ba_2TiO_4 structural units (s.u.), or "slabs," per cell. Appropriately rescaled coarser meshes were adopted for conducting ionic relaxations within larger cells that were used to approximate the influence of incommensurate lattice distortions. The density functional perturbation theory[38] (DFPT) approach was employed to compute phonon-band dispersions in Ba_2TiO_4 (again, for the tetragonal unit cell) and evaluate its structural stability. All internal ionic positions were relaxed until the forces were less than 0.4×10^{-3} Ry bohr^{-1} ($\sim$0.01 eV/Å). We simulated epitaxial thin film constraints on a cubic (001)-oriented substrate by varying the in-plane lattice constant a of the tetragonal cell and allowing the out-of-plane lattice constant c to relax (the normal stress in the out-of-plane direction was less than 0.5 kbar), while keeping the $P4/mmm$ symmetry intact. The biaxial misfit strain is defined as $\varepsilon = a/a_0 - 1$, where a_0 corresponds to the optimized lattice parameter of a structure with all the normal stresses converged to values less than 0.5 kbar. The DFPT approach was also used to compute the ionic Born effective charge tensors $Z^*_{i\alpha\beta}$ (here i is the ion number and α,β are Cartesian directions x,y,z), with the methodology outlined in Refs. 39–41 and 25, and then utilized to evaluate the phonon plasma frequencies Ω_p and the static dielectric permittivity tensor $\epsilon_{\alpha\beta}(0)$. For all polar structures, the linearized approximation involving products of $Z^*_{i\alpha\beta}$ and ionic displacements away from their centrosymmetric positions[42] was used to estimate the total electric polarization.

III. DISCUSSION

A. Structural properties

Structural parameters of the $I4/mmm$ RP Ba_2TiO_4 phase for the investigated range of biaxial strains are given in Table I, with those for the monoclinic β phase included for comparison. Both compounds are visualized in Fig. 1. Lattice constants for the nonpolar and polarized tetragonal phases of perovskite $BaTiO_3$, either relaxed to low normal stresses or constrained to the in-plane constant of the $SrTiO_3$ substrate, are also presented in the table.

TABLE I. Structural parameters for the tetragonal unit cell (see Fig. 1) of RP-type Ba_2TiO_4 at varying degrees of epitaxial strain ε. Potential substrate assignments are shown in the last column. Structural parameters obtained for nonpolar (space group $P4/mmm$) and polarized (space group $P4mm$) tetragonal phases of perovskite $BaTiO_3$ are also shown for comparison. Computed and experimental (in parentheses, taken from Ref. 11) structural parameters for β-Ba_2TiO_4 are given in the lower part of the table.

ε (%)	a (Å)	c/a	Substrate
RP-type Ba_2TiO_4 ($I4/mmm$)			
−2.426	3.851	3.469	$SrTiO_3$
−1.5	3.887	3.411	$DyScO_3$
−0.5	3.927	3.352	$SmScO_3$
0.0	3.946	3.323	$NdScO_3$
0.5	3.966	3.294	$NdScO_3$
1.5	4.006	3.239	
Perovskite $BaTiO_3$ ($P4/mmm$)			
−2.16	3.851	1.038	$SrTiO_3$
0.0	3.936	1.000	
Perovskite $BaTiO_3$ ($P4mm$)			
−1.99	3.851	1.059	$SrTiO_3$
0.0	3.923	1.012	
β-Ba_2TiO_4 ($P2_1/n$)			
a (Å)	b (Å)	c (Å)	β (deg)
6.044	7.547	10.336	94.64
(6.096)	(7.681)	(10.545)	(92.99)

The in-plane lattice constant of the unstressed RP Ba_2TiO_4 is larger than that of the nonpolar or polarized tetragonal

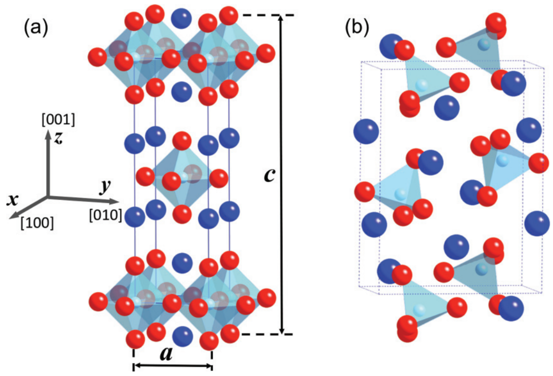

FIG. 1. (Color online) Crystal structure of the Ba_2TiO_4 compounds: (a) RP phase, space group $I4/mmm$. The a and c lattice constants for the tetragonal ($P4/mmm$) cell that contains two Ba_2TiO_4 slabs are also shown. The symmetry-equivalent slabs are connected by a body-centering translation. (b) β-orthotitanate phase, space group $P2_1/n$. TiO_6 and TiO_4 coordination cages in the RP and β phases, respectively, are represented by translucent polyhedra and Ba atoms are shown in blue (dark gray).

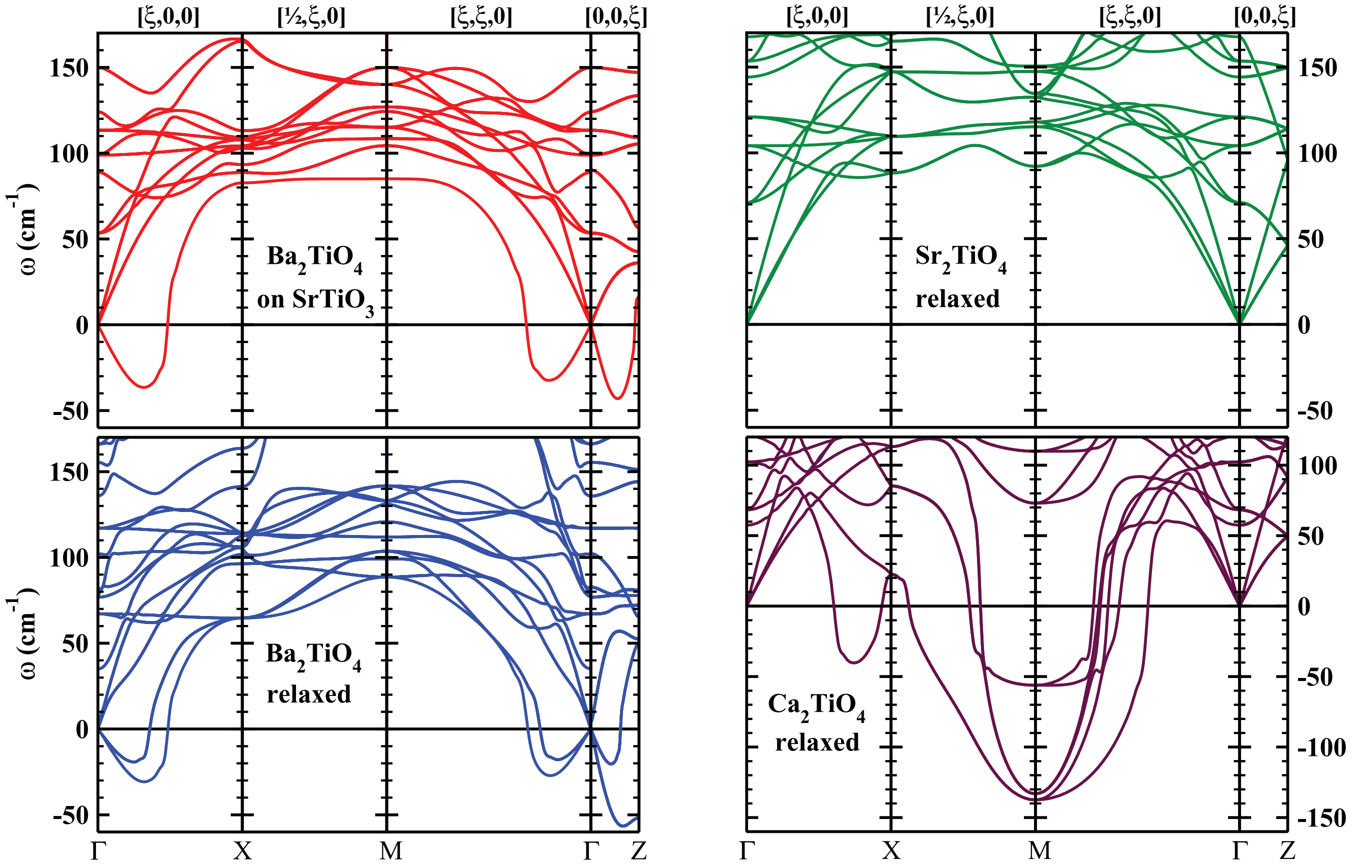

FIG. 2. (Color online) Phonon-band dispersions along some high-symmetry BZ directions in the tetragonal $P4/mmm$ unit cell of RP Ba_2TiO_4 (upper left) epitaxially matched to the $SrTiO_3$ substrate, and (lower left) relaxed to low in-plane and out-of-plane normal stresses. Dispersions along the same BZ directions are also shown for the unstressed RP Sr_2TiO_4 (upper right) and Ca_2TiO_4 (lower right). Note the different phonon frequency range in the latter plot. Imaginary frequencies associated with unstable phonon modes are plotted as negative numbers below the zero line.

$BaTiO_3$ incarnations. This puts the RP compound under a considerably higher compressive strain when matched to $SrTiO_3$ (∼2.4%), which could lead to problems during epitaxial growth on that substrate. At variance with the behavior of its ABO_3 perovskite counterpart, it is unlikely that growing RP Ba_2TiO_4 under high epitaxial compression will be beneficial for its polar properties. The rocksalt-type BaO-BaO intergrowths present in the RP structure prevent polarization formation in the out-of-plane, [001] direction,[43–45] with epitaxial "squeeze" discouraging the emergence of polar states within the xy plane.

B. Vibrations and structural stability analysis

The results of phonon-band calculations along some high-symmetry directions within the Brillouin zone of the tetragonal unit cell ($P4/mmm$ symmetry) of RP Ba_2TiO_4 are presented in Fig. 2. Phonon-band dispersions computed for the RP Ca_2TiO_4 and Sr_2TiO_4 under the same symmetry constraints are also included for comparison. Calculations for all the compounds were done along all the symmetry-inequivalent directions in the BZ (not shown). The route through the BZ along which the phonon bands are sketched in the figure is chosen to accent the main differences among the compounds—which are discussed below—rather than for the sake of computational completeness. The data not shown in the figure do not change the conclusions of this section.

It is instructive to start the discussion of these results by considering the case of Sr_2TiO_4. No vibrational instabilities were found anywhere in the BZ for this compound, confirming its stable ground state as the one possessing the $I4/mmm$ symmetry. In contrast, the data presented for Ca_2TiO_4 reveal highly pronounced structural instabilities that are the strongest around the M and A (latter not shown) points at the BZ boundary. Vibrational eigenvector analysis identifies these instabilities as antiferrodistortive octahedral cage rotations that are also predominant in the formation of the ground state of perovskite $CaTiO_3$,[46] as well as that of the higher-order Ca-based RP structures.[4,7]

In comparison to the first two compounds, the most striking feature in the phonon-band plots for both epitaxial strain states of the RP Ba_2TiO_4 is the presence of multiple unstable bands whose maximum strengths (indicated by the highest values of negative frequencies) are attained at **q** points inside the BZ, rather than at the zone center or edges. Such **q** points do not correspond to any integer number of unit cells and thus describe incommensurate (IC) modulations of the compound high-symmetry $I4/mmm$ state.[47] Furthermore, although superficially the plots for the unstressed and epitaxially strained states look similar, examination of the components of vibrational eigenvectors associated with the low-lying unstable phonon modes in each plot shows that they represent different IC structural distortions. Therefore, the character of these distortions and the resulting material ground state can be manipulated by applying the right amount of biaxial strain. The nature of the IC distortions and their strain dependence are further analyzed in the following section.

C. Analysis of incommensurate distortions

IC distortions are not rare in insulators and have been observed in a variety of oxide and fluorite materials, including a few ferroelectric compounds.[48–50] Of the latter, K_2SeO_4 (Refs. 51–54) and $NaNO_2$ (Refs. 55–61) remain as the most thoroughly studied examples during the time period spanning from the late 1970s to the early 1990s. A general theory elucidating the origins of IC distortions in insulators has been developed by Heine and McConnell,[62,63] following the mold of the standard Landau theory of second-order phase transitions.[64] According to this theory, such distortions arise due to an interaction between two or more different transformation modes that exist in the high-symmetry (undistorted) state of the system at temperatures above the IC phase transition. The transformation modes may be displacive in character (i.e., phonons), or represent a variety of ordering processes. Most importantly, their symmetries should be in a certain relation with each other in order for the interaction leading to an IC ground state to take place. Specifically, the mode symmetries at a high-symmetry $\mathbf{q}$ point $\tilde{\mathbf{q}}$, such as the BZ center or edge, should be different, prohibiting mode interaction at this point. However, at more generic points within the vicinity of $\tilde{\mathbf{q}}$, the reduced mode symmetries should be the same, allowing the modes to interact with each other. In the same fashion as for electronic states, the interaction then bends the upper band up and the lower band down, and the shape of the latter develops a downward "hump" with a minimum at an IC value of $\mathbf{q}$. When this effect is strong enough, e.g., when the mode frequencies are close together, the minimum of the lower band can fall below the zero line, producing an IC structural instability, like the ones shown in the left panels of Fig. 2. The relation connecting the symmetries of the modes is automatically satisfied when one mode is even and the other one is odd with respect to some symmetry operation—such as, for example, a center of inversion—belonging to the symmetry group of $\tilde{\mathbf{q}}$.

In the upper part of Fig. 3 we present evolution of the low-frequency phonon bands in the RP Ba_2TiO_4 under varying epitaxial strain (from 2.43% compression on the $SrTiO_3$ substrate to 1.5% tension) along the Γ-Λ-Z path within the BZ of its $P4/mmm$ unit cell. As shown in Fig. 2, this is the direction along which the strongest structural instabilities are found. The symmetries of the bands, or the irreducible representations (irreps) according to which they transform, for all the symmetry-inequivalent $\mathbf{q}$ points on the path are collected in Table II. In the lower part of Fig. 3 we show crude sketches of distortions produced by combinations of frozen-in IC and polar instabilities along the Γ-Λ-Z BZ path. Atomic-level animations for some of the unstable vibrational modes (or combinations thereof) corresponding to the sketches above are included as a Supplemental Material for this paper.[65]

Two pairs of phonon bands can be identified from Fig. 3 and Table II that satisfy the symmetry relation of Heine and McConnell[62,63] for the formation of the IC state. One such pair includes nondegenerate bands **a** and **d**. The associated phonon modes transform according to irreps A_{1g} and A_{2u}, respectively, at Z, and irrep A_1 at Λ. Examination of the mode eigenvectors at Z reveals that they represent vibrations of individual Ba_2TiO_4 slabs along the [001] direction, which are either even (A_{1g}) or odd (A_{2u}) with respect to an inversion point in the center of the unit cell that is doubled along [001]. Eigenvector visualization at $\xi = \frac{1}{3}, \frac{1}{4}$, and $\frac{1}{5}$—i.e., for supercells made up of three, four, and five original unit cells in the [001] direction—shows distortion motifs that resemble mixtures of the pure vibrations A_{1g} and A_{2u} at Z. Band **a**, which comprises the lower branch of the pair for all strains except high tensions, remains unstable at $\varepsilon \sim (-2.5,0.0)\%$ and dominating in strength at compressive strains higher than approx. 1.5% (see Fig. 3). Throughout its unstable strain interval, this band forms a minimum, with $\xi_{\min} \simeq \frac{3}{10}$ at $\varepsilon \sim (-2.5, -1.5)\%$. We conclude that for these strain values the low-temperature state of the system will be governed by a lattice distortion consisting of a series of displacements of individual Ba_2TiO_4 slabs away from the their high-symmetry $I4/mmm$ positions along [001] with a period that is slightly longer than three unit cells.

The other pair of transformations satisfying the symmetry criteria of Refs. 62 and 63 includes doubly degenerate bands **b** and **c**, with the associated phonon modes transforming according to irreps E_g and E_u, respectively, at Z, and irrep E at Λ. Analysis of their eigenvectors at Z demonstrates that these modes correspond to individual Ba_2TiO_4 slabs sliding with respect to each other in the xy plane, again with displacement patterns that are even (E_g) or odd (E_u) with respect to inversion through the center of the unit cell doubled along [001]. Mode eigenvector visualization for *commensurate* values of ξ, equivalent to supercells made of three, four, and five unit cells in the [001] direction, again shows displacement motifs that resemble mixtures of the aforementioned pure E_g and E_u modes at Z. Band **b**, which comprises the lower branch of the pair, becomes unstable at compressive strain of approx. 1.5% and remains unstable for all the explored strain states that are more tensile. It develops a stronger instability than the band **a** at $\varepsilon \sim -0.5\%$, forming a minimum at the value of $\xi_{\min}$ that is close, but not exactly equal, to $\frac{1}{3}$. As depicted in Fig. 3, this IC distortion dominates the energy landscape of the system for the strain interval of approx. $(-0.5,0.5)\%$.

TABLE II. Phonon band symmetries along the Γ–Z path in the Brillouin Zone of the $P4/mmm$ unit cell of the RP Ba_2TiO_4.

Band in Fig. 3	Γ (0, 0, 0) $4/mmm$	Λ (0, 0, ξ) $4mm$	Z (0, 0, $\frac{1}{2}$) $4/mmm$
a (red)	A_{2u}	A_1	A_{1g}
b (blue)	E_u	E	E_g
c (maroon)	E_u	E	E_u
d (violet)	A_{2u}	A_1	A_{2u}
e (black)	E_g	E	E_u
f (dark green)	E_u	E	E_u
g (light green)	E_u	E	E_g

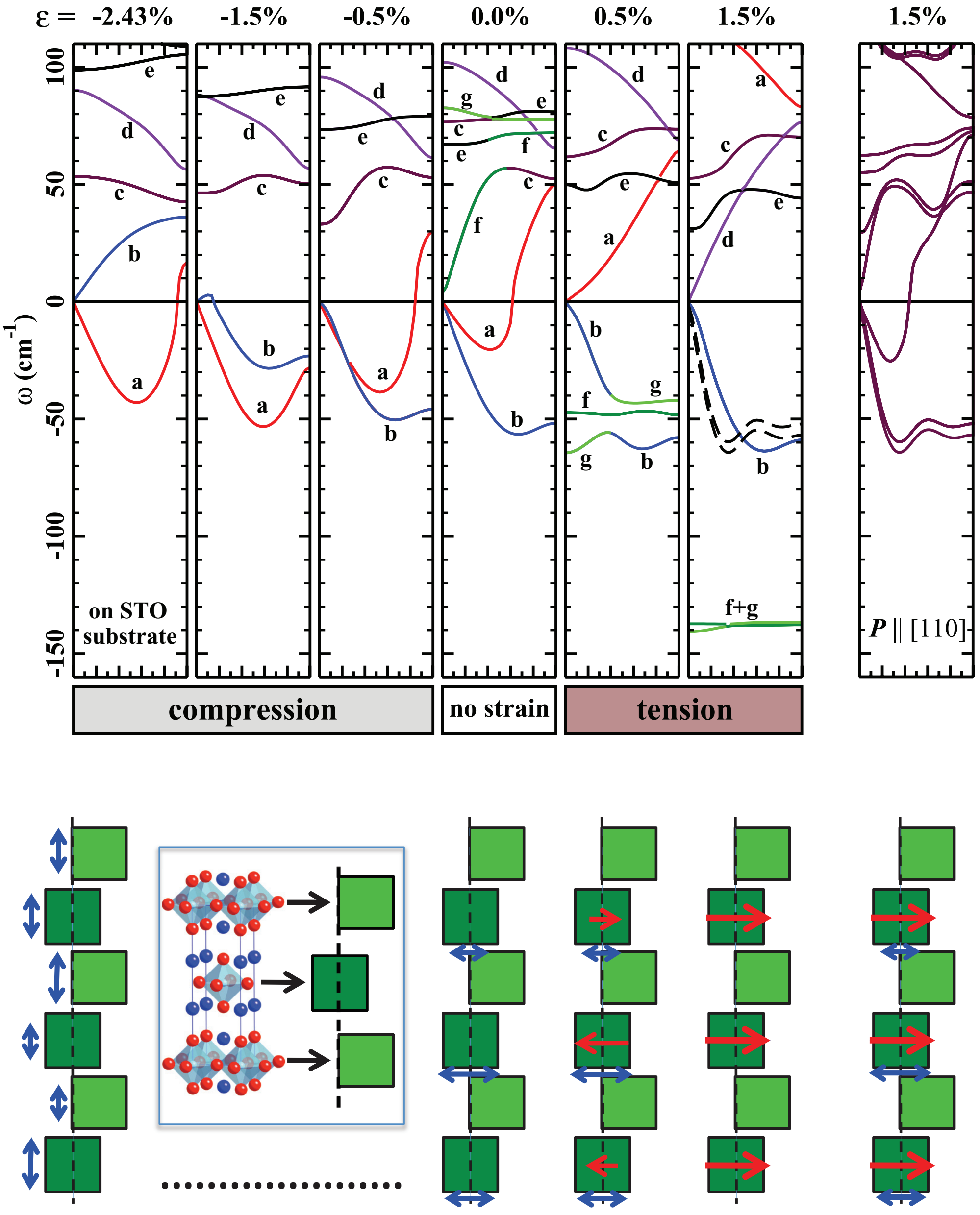

FIG. 3. (Color online) Top: Evolution of the low-lying Γ-*Z* phonon bands in the epitaxial $I4/mmm$ RP structures with respect to varying biaxial strain ε. Imaginary frequencies associated with unstable modes are plotted as negative numbers below the horizontal zero line. See Table II for the band symmetry assignments. Phonon bands for the $Amm2$ structure at $\varepsilon = 1.5\%$ with developed polarization along the [110] direction are shown in the rightmost panel. The dominant IC instabilities in the polar structure are also drawn in dashed lines in the neighboring panel containing the data for its high-symmetry counterpart. Bottom: Sketches of IC and polar distortions that correspond to the situations depicted in the phonon-band panels in the upper part of the figure. For any specific value of ε an appropriate sketch is located directly under the phonon-band structure plot. Double-ended (blue) arrows indicate varying amplitudes of the IC vibrations of individual Ba_2TiO_4 slabs, while single-ended (red) arrows represent polar distortions within the slabs. See the text for more details.

The last ingredients that factor into the determination of the ground state of the system are doubly degenerate bands **f** and **g** that are characterized by strong polar distortions of the TiO_6 octahedra in the xy plane at all the **q** points along the Γ-Λ-*Z* BZ path. At the Γ point these modes correspond, respectively, to antiferroelectric (AFE) and ferroelectric (FE) distortions within the $P4/mmm$ unit cell. As shown in Fig. 3, these bands start to soften up around $\varepsilon \sim 0.0\%$ and at tensile strains of 0.5% and larger they become unstable. For high tensile strain of 1.5%, the polar instabilities are much stronger than the IC ones and have no dispersion along the chosen BZ path. Under such strain, we would expect the ground state of the system to be *commensurate* and polar (see further discussion below). However, for intermediate tensile strain of 0.5%, the polar and IC instabilities have similar strengths. Furthermore, since at a generic **q** point Λ their symmetries are the same, they strongly mix with each other (see the "$\varepsilon = 0.5\%$" panel in Fig. 3). Visualization of the eigenvectors of such modes for the commensurate values of ξ shows displacement patterns similar to those of the planar IC vibrations discussed in the preceding paragraph, but with individual Ba_2TiO_4 slabs simultaneously exhibiting strong polar distortions that are uncorrelated in direction among the neighboring slabs.

Finally, in order to evaluate the influence of developing in-plane polarization on IC distortions, we have frozen the dominating Γ-point FE instability into the $I4/mmm$ structure at $\varepsilon = 1.5\%$. The preferred polarization orientation within the xy plane was found to be along the [110] direction, which reduced the symmetry of the initial nonpolar structure to polar space group $Amm2$. The magnitude of in-plane polarization in the polar structure relaxed under the same epitaxial constraints as the non-polar one was found to be $0.17\ \mathrm{C/m^2}$. Phonon bands computed for this structure along the Γ-Λ-Z BZ path are shown in the rightmost panel of Fig. 3. As expected, polar instabilities (such as bands **f** and **g** in the original structure) are no longer present here, as the associated structural distortions froze in during the symmetry-lowering phase transition. Nevertheless, the developing polarization did not eliminate the IC instabilities, which are still present in the plot at about the same strength as in the nonpolar structure, but with $\xi_{\min} \simeq 0.15$. Therefore the resulting structure did not lock into a commensurate polar state. Visualization of the eigenvectors of the unstable bands remaining in the $Amm2$ structure (which are no longer degenerate due to reduced symmetry) for the commensurate values of ξ shows [110]-polarized Ba_2TiO_4 slabs shifting with respect to each other in the xy plane.

Utilizing the same strategies it should be possible to analyze structural distortions produced by IC modes that become unstable in other areas within the BZ (see the left panels of Fig. 2). As the dominant Γ-Z instabilities described above condense, these "sidekick" modes can interact with them constructively, by freezing in together, or destructively, by having their frequencies hardened into the realm of *stable* vibrations. However, in any case, compared to the dominant modes, the influence of any such distortions on the system structure will be much weaker and, as shown in the next section, their energy contributions to its stability will be negligible. Due to the prohibitively large sizes of the supercells that will have to be used in the further structural and vibrational analysis of the IC distorted RP compounds, we have not explored the issues related to condensation of the sidekick IC instabilities any further. Nevertheless, this does not prevent us from drawing some conclusions (outlined below) about the transitional behavior of these materials.

D. Total energy comparisons

In Fig. 4 we present the comparison of total energies computed for all of the epitaxial RP and for the β Ba_2TiO_4 structures within the DFT-LDA framework used in this paper.[66] In the top panel, the energy change due to the applied epitaxial strain is shown for the $I4/mmm$ structures, with the energy of the structure relaxed to low normal stresses taken as zero. The energy of the $P2_1/n$ β phase is 223 meV/s.u. higher than the energy of the latter. The energies of the epitaxial RP structures exhibit a roughly parabolic dependence on the magnitude of the applied strain and, with the exception of the highly compressed state on the $SrTiO_3$ substrate, are less than 100 meV/s.u. above the energy of the reference unstressed structure.

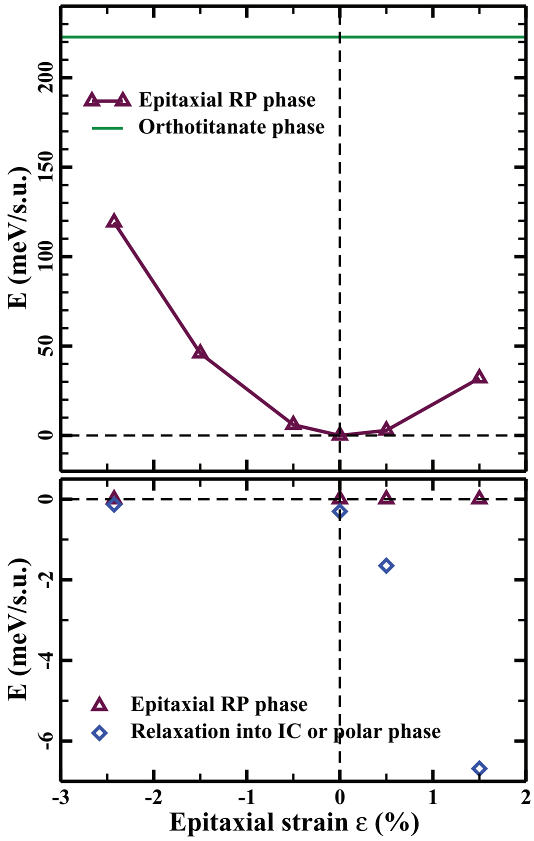

FIG. 4. (Color online) Top: Total energy dependence on the epitaxial strain ε for the undistorted ($I4/mmm$) RP structures. The energy of the unstressed structure is taken as zero. Data for the $P2_1/n$ β-orthotitanate phase are also shown for comparison. Bottom: Total energy decrease in the epitaxial RP structures after freezing in the leading structural instabilities. The total energies of the $I4/mmm$ configurations are taken as zeros for each strain state.

In the lower panel of the same figure, taking the energy of each $I4/mmm$ epitaxial RP structure as zero, we show the reduction of the total energy after allowing the dominating structural instability—be it IC, polar, or the combination of the two in the case of $\varepsilon = 0.5\%$—to relax during the symmetry-lowering phase transition. To make calculations of the energies of the IC configurations tractable, we used supercells corresponding to the commensurate values of ξ nearest to $\xi_{\min}(\varepsilon)$. As can be seen from the plot, stabilization energies for purely IC distortions that occur at compressive strains are quite small, being on the order of a few tenths of a meV/s.u. At tensile strains, when either mixed or purely polar distortions dominate, stabilization energies increase to a few meV/s.u., following the growing strength of the polar instabilities that are being frozen into the high-symmetry structure.

The total energy changes due to epitaxial strain and the following polar distortions in the RP Ba_2TiO_4 structures are similar to those obtained for perovskite $BaTiO_3$. For the latter, the energy difference between the nonpolar $P4/mmm$ phases grown on $SrTiO_3$ and relaxed to low normal stresses is 85 meV/s.u., while the stabilization energies due to a distortion

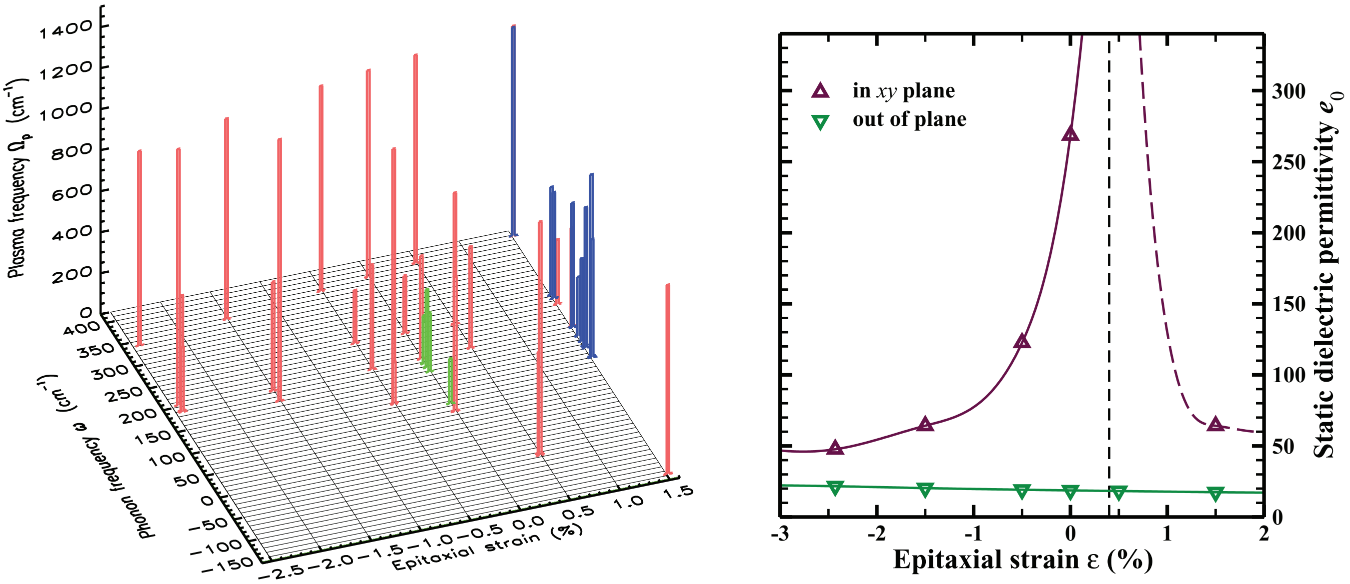

FIG. 5. (Color online) Left: Variation of vibrational frequencies ω and phonon plasma frequencies Ω_p of the optical polar modes in the epitaxial $I4/mmm$ RP Ba_2TiO_4 structures with respect to biaxial strain ε. Again, imaginary phonon frequencies associated with unstable modes are plotted as negative numbers below the zero line. Data set shown in green (light gray) at $\varepsilon = 0.0\%$ represents the plasma frequencies of the $P2_1/n$ β-Ba_2TiO_4 structure. An extra blue (dark gray) data set at $\varepsilon = 1.5\%$ shows the plasma frequencies of the polar $Amm2$ structure. Right: In-plane and out-of-plane components of the static dielectric susceptibility tensor computed for the RP Ba_2TiO_4 structures with respect to biaxial strain ε. At compressive and zero strains the data points on the plot for the in-plane component are computed for the nonpolar $I4/mmm$ structures, while the one at tensile strain is obtained for the polar $Amm2$ structure. Lines connecting the data points are used as a guide to the eye.

into the polar $P4mm$ phase are 7 and 33 meV/s.u. for the relaxed and grown-on-$SrTiO_3$ epitaxial conditions, respectively.

E. Dielectric properties

We have evaluated the dielectric properties of the epitaxial RP Ba_2TiO_4 structures by computing their phonon plasma frequencies Ω_p and the in-plane and out-of-plane components of their static dielectric permittivity tensors. The results of our calculations are presented in Fig. 5. Plasma frequencies can be computed for both stable and unstable vibrations, and at least two major branches of modes with high Ω_p are identified in the $I4/mmm$ RP compounds for $\omega \leqslant 400$ cm^{-1} at varying epitaxial strain [see the red (medium gray) columns in the left panel of Fig. 5]. The lower branch has a strong dependence on ε, becoming soft in epitaxial tension, while the upper one remains relatively flat throughout the interval of studied strains. The extra data shown in the same panel in blue (dark gray) for $\varepsilon = 1.5\%$ illustrate the changes in the distribution of the high-plasma-frequency modes upon the transition from the nonpolar $I4/mmm$ to the polar $Amm2$ phase, with the main difference of an unstable mode at $\omega \simeq 140i$ cm^{-1} being eliminated. Plasma frequencies for the monoclinic β phase, shown in green (light gray) at $\varepsilon = 0.0\%$, are also included for comparison.

The components of the static dielectric permittivity tensors, shown in the right panel of Fig. 5, were computed for the $I4/mmm$ structures at compressive and zero strains, and for the $Amm2$ structure at the tensile strain of 1.5% (no Γ-point instabilities are present in all these structures). The tensile strain of 0.5% belongs to the transition area where the frequencies of the Γ-point polar modes start to fall through the zero line, and the in-plane component of the permittivity tensor in that region is assumed to be large. This divergence is sketched in the panel by solid and dashed lines. The largest value of the in-plane component of the permittivity tensor that was actually computed is ~270, which should be achievable in RP structures at small epitaxial strains, e.g., on the $NdScO_3$ substrate (see Table I). Due to the suppression of the out-of-plane low-frequency polar vibrations in the RP structures, the associated permittivity tensor component remains small throughout the whole interval of studied strains.

IV. CONCLUSIONS

By studying the vibrations, structural stability, and polar properties of the RP-type Ba_2TiO_4 phase subject to a range of epitaxial strains, we find IC distortions in its structure that evolve depending on the magnitude of the applied strain. In-plane or out-of-plane oriented IC modes could condense, either separately or in combination with polar modes of the same symmetry, producing a variety of complicated structural arrangements. The existence of IC instabilities in RP Ba_2TiO_4 is in compliance with the theory of Heine and McConnell.[62,63] However, in a usual case, such as $NaNO_2$, the IC phase forms as an intermediate layer separating *commensurate* nonpolar high-temperature and polar low-temperature phases. In the case considered here, IC distortions are a part of the ground state of the system at 0 K. Because of the tiny energy contributions to the system stability produced by these distortions, they could be washed out at temperatures of just a few kelvin, leaving behind a commensurate $I4/mmm$ nonpolar (epitaxial compression) or $Amm2$ polar (epitaxial tension) state. Structures grown at epitaxial conditions that are close to the nonpolar-to-polar structural transition boundary—tensions of a few tenths of a %—have large in-plane static dielectric constants, while those grown in higher tension have smaller dielectric constants and a developed in-plane polarization on the order of 0.17 C/m^2.

The peculiar properties of the RP Ba_2TiO_4 phase originate from the need to accommodate the heavy and bulky Ba ions within this structure. In the RP Sr_2TiO_4, low-lying Γ-Z phonon modes have exactly the same symmetries and, based on their eigenvector visualization, produce similar-looking displacement motifs. However, in Sr_2TiO_4 the bands representing the vibrations of the perovskite slabs are stiffer, as well as much more dispersive (see the top right panel in Fig. 2). The increased vibrational frequencies of such motions could be the simple consequence of the lightness of the Sr- rather than Ba-based slabs, while the exact mechanism behind the suppression of the downward-hump development in the lower phonon bands still has to be fully revealed. On the other hand, the phonon-band dispersions in the RP Ba_2TiO_4 epitaxially matched to $SrTiO_3$ (top left panel in Fig. 2) look remarkably similar to those of Sr_2TiO_4, with the exception of just one band splitting down and forming unstable pockets along a number of directions within the BZ.

In this investigation we have shown that respectable dielectric and polar properties could be induced in the RP Ba_2TiO_4 grown under slight to moderate epitaxial tension, which could be realized on some Sc-based substrates. The energy analysis within the DFT-LDA framework presented here indicates that epitaxial RP phases are likely to form over the monoclinic β phase. In the companion paper (Ref. 32) we also (i) conduct a detailed analysis of energetics of both RP and β structural configurations, showing that there is more depth to this story, and (ii) evaluate and compare the geometrical openness of these polymorphs in preparation for the studies of their molecular-absorption properties.

ACKNOWLEDGMENTS

This project was supported by the US Department of Energy, Office of Science, Office of Basic Energy Sciences and by American Recovery and Reinvestment Act (ARRA) funding through the Office of Advanced Scientific Computing Research under Contract No. DE-AC02-06CH11357. S.M.N. is grateful to the members of the Department of Dielectrics, Institute of Physics, the Academy of Sciences of the Czech Republic (Prague), for their hospitality during his visit to the institute in the spring of 2012. S.M.N. would also like to thank Jiří Hlinka and Jan Petzelt for illuminating discussions on the nature of incommensurate distortions in oxides, and Peter Littlewood for bringing the work of Heine and McConnell to his attention.

---

[1] S. N. Ruddlesden and P. Popper, Acta Crystallogr. **10**, 538 (1957).
[2] S. N. Ruddlesden and P. Popper, Acta Crystallogr. **11**, 54 (1958).
[3] G. Burns, F. H. Dacol, G. Kliche, W. König, and M. W. Shafer, Phys. Rev. B **37**, 3381 (1988).
[4] M. M. Elcombe, E. H. Kisi, K. D. Hawkins, T. J. White, P. Goodman, and S. Matheson, Acta Crystallogr., Sect. B **47**, 305 (1991).
[5] J. H. Haeni, C. D. Theis, D. G. Schlom, W. Tian, X. Q. Pan, H. Chang, I. Takeuchi, and X.-D. Xiang, Appl. Phys. Lett. **78**, 3292 (2001).
[6] W. Tian, X. Q. Pan, J. H. Haeni, and D. G. Schlom, J. Mater. Res. **16**, 2013 (2001).
[7] B. V. Beznosikov and K. S. Aleksandrov, Kristallografiya (Crystallogr. Rep.) **45**, 792 (2000).
[8] R. V. Shpanchenko, E. V. Antipov, and L. M. Kovba, Zh. Neorg. Khim. **38**, 599 (1993).
[9] P. R. Slater and R. K. B. Gover, J. Mater. Chem. **11**, 2035 (2001).
[10] J. A. Bland, Acta Crystallogr. **14**, 875 (1961).
[11] K. K. Wu and I. D. Brown, Acta Crystallogr., Sect. B **29**, 2009 (1973).
[12] J. R. Günter and G. B. Jameson, Acta Crystallogr., Sect. C **40**, 207 (1984).
[13] G. Pfaff, J. Mater. Sci. Lett. **10**, 1059 (1991).
[14] G. Pfaff, J. Mater. Chem. **2**, 591 (1992).
[15] S. J. Lee, M. D. Biegalski, and W. M. Kriven, J. Mater. Res. **14**, 3001 (1999).
[16] T. Ahmad and A. K. Ganguli, J. Mater. Res. **19**, 2905 (2004).
[17] D. Guo, T. Goto, C. Wang, Q. Shen, and L. Zhang, Mater. Lett. **70**, 135 (2012).
[18] A. Ito, D. Guo, R. Tu, and T. Goto, Mater. Chem. Phys. **133**, 398 (2012).
[19] H. Marusawa and Y. Saito, Key Eng. Mater. **350**, 143 (2007).
[20] Y. Saito, H. Sato, and Y. Sakabe, J. Chem. Eng. Jpn. **41**, 441 (2008).
[21] R. Inoue, S. Ueda, K. Wakuta, K. Sasaki, and T. Ariyama, ISIJ Int. **50**, 1532 (2010).
[22] V. Shanker, T. Ahmad, and A. K. Ganguli, Bull. Mater. Sci. **27**, 421 (2004).
[23] T. Hungría and A. Castro, J. Alloys Compd. **436**, 266 (2007).
[24] *Physics of Ferroelectrics: A Modern Perspective*, edited by K. M. Rabe, C. H. Ahn, and J.-M. Triscone,Topics in Applied Physics Vol. XII (Springer-Verlag, Berlin, 2007).
[25] C. J. Fennie and K. M. Rabe, Phys. Rev. B **68**, 184111 (2003).
[26] N. D. Orloff, W. Tian, C. J. Fennie, C. H. Lee, D. Gu, J. Mateu, X. X. Xi, K. M. Rabe, D. G. Schlom, I. Takeuchi, and J. C. Booth, Appl. Phys. Lett. **94**, 042908 (2009).
[27] W. Wunderlich and K. Koumoto, Int. J. Mater. Res. **97**, 657 (2006).
[28] Y. Wang, K. H. Lee, H. Hyuga, H. Kita, K. Inaba, H. Ohta, and K. Koumoto, Appl. Phys. Lett. **91**, 242102 (2007).
[29] Y. Wang, K. H. Lee, H. Ohta, and K. Koumoto, J. Appl. Phys. **105**, 103701 (2009).
[30] A. Chernatynskiy, R. W. Grimes, M. A. Zurbuchen, D. R. Clarke, and S. R. Phillpot, Appl. Phys. Lett. **95**, 161906 (2009).
[31] P. A. Salvador, T.-D. Doan, B. Mercey, and B. Raveau, Chem. Mater. **10**, 2592 (1998).
[32] W. D. Parker and S. M. Nakhmanson (unpublished).
[33] D. M. D'Alessandro, B. Smit, and J. R. Long, Angew. Chem. Int. Ed. **49**, 6058 (2010).

[34] P. Giannozzi, S. Baroni, N. Bonini, M. Calandra, R. Car, C. Cavazzoni, D. Ceresoli, G. L. Chiarotti, M. Cococcioni, I. Dabo, A. D. Corso, S. de Gironcoli, S. Fabris, G. Fratesi, R. Gebauer, U. Gerstmann, C. Gougoussis, A. Kokalj, M. Lazzeri, L. Martin-Samos, N. Marzari, F. Mauri, R. Mazzarello, S. Paolini, A. Pasquarello, L. Paulatto, C. Sbraccia, S. Scandolo, G. Sclauzero, A. P. Seitsonen, A. Smogunov, P. Umari, and R. M. Wentzcovitch, J. Phys.: Condens. Matter **21**, 395502 (2009).

[35] J. P. Perdew and A. Zunger, Phys. Rev. B **23**, 5048 (1981).

[36] D. Vanderbilt, Phys. Rev. B **41**, 7892 (1990).

[37] H. J. Monkhorst and J. D. Pack, Phys. Rev. B **13**, 5188 (1976).

[38] S. Baroni, S. de Gironcoli, A. Dal Corso, and P. Giannozzi, Rev. Mod. Phys. **73**, 515 (2001).

[39] G.-M. Rignanese, X. Gonze, and A. Pasquarello, Phys. Rev. B **63**, 104305 (2001).

[40] G.-M. Rignanese, F. Detraux, X. Gonze, and A. Pasquarello, Phys. Rev. B **64**, 134301 (2001).

[41] X. Zhao and D. Vanderbilt, Phys. Rev. B **65**, 075105 (2002).

[42] S. M. Nakhmanson, K. M. Rabe, and D. Vanderbilt, Appl. Phys. Lett. **87**, 102906 (2005).

[43] S. M. Nakhmanson, Phys. Rev. B **78**, 064107 (2008).

[44] S. M. Nakhmanson and I. Naumov, Phys. Rev. Lett. **104**, 097601 (2010).

[45] E. Bousquet, J. Junquera, and P. Ghosez, Phys. Rev. B **82**, 045426 (2010).

[46] K. Parlinski, Y. Kawazoe, and Y. Waseda, J. Chem. Phys. **114**, 2395 (2001).

[47] X. Gonze, R. Caracas, P. Sonnet, F. Detraux, P. Ghosez, I. Noiret, and J. Schamps, in *Fundamental Physics of Ferroelectrics 2000*, edited by R. E. Cohen, AIP Conf. Proc. No. **535** (AIP, New York, 2000), p. 163.

[48] J. Petzelt, Phase Transitions **2**, 155 (1981).

[49] T. Janssen and A. Janner, Adv. Phys. **36**, 519 (1987).

[50] H. Z. Cummins, Phys. Rep. **185**, 211 (1990).

[51] M. Iizumi, J. D. Axe, G. Shirane, and K. Shimaoka, Phys. Rev. B **15**, 4392 (1977).

[52] V. Dvořák and J. Petzelt, J. Phys. C **11**, 4827 (1978).

[53] J. Petzelt, G. V. Kozlov, A. A. Volkov, and Y. Ishibashi, Z. Phys. B **33**, 369 (1979).

[54] M. S. Haque and J. R. Hardy, Phys. Rev. B **21**, 245 (1980).

[55] K. H. Michel and J. Fivez, Ferroelectrics **36**, 289 (1981).

[56] K. H. Michel, Phys. Rev. B **24**, 3998 (1981).

[57] J. Fivez and K. H. Michel, Z. Phys. B **51**, 127 (1983).

[58] R. M. Lynden-Bell, M. L. Klein, and I. R. McDonald, Z. Phys. B **54**, 325 (1984).

[59] V. Heine, R. M. Lynden-Bell, J. D. C. McConnell, and I. R. McDonald, Z. Phys. B **56**, 229 (1984).

[60] A. Yamamoto, Phys. Rev. B **31**, 5941 (1985).

[61] U. Bianchi, W. Kleemann, D. Sommer, Y. S. Cho, J. G. Yoon, and S. I. Kwun, Phase Transitions **36**, 145 (1991).

[62] J. D. C. McConnell, Am. Mineral. **68**, 1 (1983).

[63] V. Heine and J. D. C. McConnell, J. Phys. C **17**, 1199 (1984).

[64] L. D. Landau and E. M. Lifshitz, *Statistical Physics, Part I*, Course of Theoretical Physics Vol. 5 (Butterworth-Heinemann, London, 1980).

[65] See Supplemental Material at http://link.aps.org/supplemental/10.1103/PhysRevB.88.035203 for JMOL animations of the vibrational modes. The included animations correspond to the four distortion sketches of the centrosymmetric $I4/mmm$ RP structure shown in the bottom part of Fig. 3 for $\varepsilon = -2.43\%, 0.0\%, 0.5\%$, and 1.5%. JMOL is an open-source Java viewer for chemical structures in three dimensions. http://www.jmol.org/ .

[66] For a more detailed total energy comparison between the RP and β-Ba_2TiO_4 structures see Ref. 32.